33RD CONGRESS
OF THE INTERNATIONAL COUNCIL
OF THE AERONAUTICAL SCIENCES
STOCKHOLM, SWEDEN, 4-9 SEPTEMBER, 2022

ICAS 2022 SWEDEN

# Overview of Aerodynamic Design Activities Performed at ONERA to Reduce Aviation's climate impact

M. Méheut[1], G. Arnoult[1], O. Atinault[1], Q. Bennehard[1], C. François[1]

[1]*ONERA, Université Paris-Saclay, 8 Rue des Vertugadins, 92190, Meudon, France.*

## Abstract

This paper aims at summarizing the recent aerodynamic design activities performed at ONERA on promising innovative aircraft and engine integration concepts with the objective to strongly reduce Aviation's climate impact. Within different projects of the Clean Sky 2 European Programme, ONERA explores two specific aircraft configurations combined with two innovative engine integration technologies for a typical Small Medium Range (SMR) mission. Three concepts are proposed in this paper with three different targets in terms of entrance into service (2035, 2045, 2050+).

First, a summary of first aerodynamic optimizations based on Overall Aircraft inputs for a High Aspect Ratio Strut-Braced Wing (HAR SBW) concept performed in the frame of the U-HARWARD project is proposed. The results show important potential benefits compared to a classical cantilever wing. Then, aerodynamic design and optimization studies on a Blended Wing Body concept are described with a two step approach: the design of the glider configuration first and then a derivative configuration with Boundary Layer ingestion. The synergy between the aircraft concept and this innovative engine integration technology underlines important potential benefits in terms of aerodynamic performance. Finally, the aerodynamic design of an hybrid electric concept equipped with distributed propulsion is described. The integration of such engine concept is very challenging in transonic conditions, a first configuration is proposed with a proper aerodynamic behavior.

## 1. General Introduction

The reduction of the environmental footprint of aviation and its impact on climate change is today the main challenge of the aeronautical industry. In this context, the European Commission has defined very ambitious objectives in the “Fligthpath 2050” vision [1] to go towards carbon free aircraft configuration. It includes 75% reduction of $CO_2$ and 90% reduction of $NO_x$ emissions, as well as a 65% reduction of noise. The only solution to achieve these very challenging targets is to integrate innovative technologies on future aircraft with radical modifications of the aircraft and engine architectures (together with the engine integration).

For that purpose, ONERA proposes in this paper an overview of aerodynamic design activities on three different disruptive concepts with three targets in terms of aircraft entrance into-service (EIS 2035, 2045, 2050+). The first configuration with a short term vision (2035) is the High-Aspect Ratio Strut-Braced Wing (HAR SBW) which enables significant increase of the wing aspect ratio (AR) to improve overall aircraft performances through aerodynamic efficiency gains without tremendous wing weight increase that a cantilever wing of similar AR would suffer from [2]. In the frame of the Clean Sky 2 U-HARWARD, ONERA is responsible for the conceptual and detailed aerodynamic designs of this concept [3]. In §2, a summary of the first results is proposed with a brief description of the main OAD results and of the aerodynamic optimization performed at the optimal AR value (19).

For the medium/long term vision (EIS 2045), the Blended Wing Body (BWB) configuration seems one of the most promising concept for a SMR mission [4]. The greater interior volume offered by the BWB geometry is a

key advantage to explore new propulsion sources such as hydrogen. Moreover, it offers potential important synergies with disruptive engine integration such as Boundary Layer Ingestion (BLI) [5][6][7] and Distributed Propulsion (DP). In the frame of the Clean Sky 2 NACOR project, ONERA performed detailed aerodynamic design of the glider and BLI BWB configurations [8][9] based on conceptual design outputs [10]. §3 summarizes all these aerodynamic activities.

For the longer term vision (2050+), the hybrid and 100% electric concepts are very promising to go towards carbon free aircraft configurations. In the frame of the Clean Sky 2 ADEC project, ONERA developed the DRAGON concept to have an estimation of the potential benefits of hybrid electric according to battery efficiency [11][12]. In this context, a first challenging detailed aerodynamic design (on a 2.5D wing section) was performed and is summarized in §4 in transonic conditions.

## 2. The Strut-Braced-Wing concept

In the project U-HARWARD [3], ONERA in collaboration with the other partners investigates the potential of the HAR-SBW concept at aircraft level (see §2) for a A321-LR like mission but also in terms of aerodynamic performance (see §2.1). In this context, a high-fidelity aerodynamic analysis and design approach has been developed to evaluate the HAR-SBW aerodynamic benefits. A detailed analysis of the optimized configuration as well as the different design steps are detailed hereafter.

### 2.1 Aerodynamic Computational process

The computational chain used in this work is an adaptation of the Computational Aircraft Prototype Syntheses (CAPS) chain developed at MIT [13] which connects different Analysis Interface Modules (AIM), as illustrated in Figure 8. In the SBW and BWB studies (see §3), four AIM are used to automatically generate a CFD mesh and perform CFD simulations.

First, the chain includes a fully parametric Computer Aided Design (CAD) module: the open source software Engineering Sketch Pad (ESP) tool developed by MIT [14]. The parameters used to define the aerodynamic shape can then be directly used as design variables of an optimization problem. Furthermore, as it possesses a CAD engine based on Open Cascade, ESP can easily compute the volumes and intersections of complex forms, allowing to easily handle geometrical constraints such as internal volume constraint.

Second, an inviscid or viscous unstructured mesh can be generated automatically on the geometry, leveraging Pointwise scripts [15]. The boundary layer refinement is ensured using the T-Rex capability of Pointwise, in the case of RANS CFD computations.

On these unstructured meshes, different CFD simulation tools can be used to solve the aerodynamic field around the shape. The current chain is compatible with the elsA software (ONERA-Airbus-Safran property) [16] as well as with the open source flow solver SU2 [17]. The CFD software are able to perform both Euler and RANS modelling of the flow. The Spalart-Allmaras turbulence model is used with both software.

Finally, the in-house ONERA post process tool *ffd* (far-filed drag analysis) [18] is employed to extract and decompose the drag coefficients of the shape into wave, induced and viscous components and remove the spurious drag inherent to the numerical modelling of the flow. These four steps are run automatically thanks to Python scripts, adapted from the CAPS chain.

### 2.2 Reference SBW aircraft

The ONERA overall design process, FAST-OAD, was applied to assess and validate the performance of the reference Tube and Wing (TW) configuration (A321-LR) as well as the reference SBW configuration, the ONERA ALBATROS concept [2]. The geometry of the A321-LR aircraft is gradually modified to reach, in the end, the geometry of the ALBATROS aircraft. The first modification consists in moving the engines from under the wing to the rear aircraft and modelling a T-Tail geometry, to ensure the efficiency of the horizontal plane. All details are explained in [3].

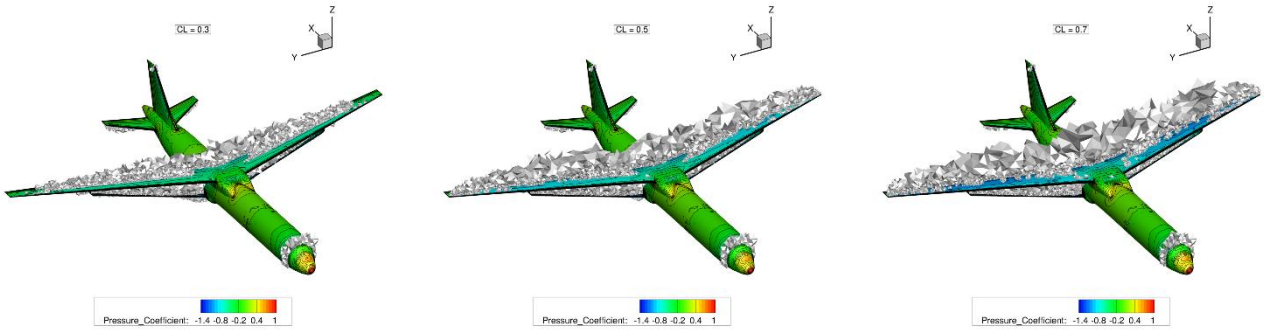


**Figure 1. Strut-Braced Wing - Wave drag sources based on Euler simulations on the reference Strut-Braced Wing configuration [3].**

## 2.3 Influence of the Aspect Ratio on the SBW performance at aircraft level

Based on the OAD process described in [3] a parametric study was achieved at conceptual level to analyze the aero-structural compromises and determine the optimal AR for the SBW concept in terms of fuel consumption. Several geometries of the SBW configuration are considered for various aspect ratio $AR \in [10, 12, 14, 16, 18, 20, 22]$ in combination with the position of the junction between the strut and the wing in the spanwise direction $\eta_{strut} = \frac{y_{junction}}{b}$.

The quantities of interest are the MTOW, the block fuel and the wing weight which are expected to decrease compared to a cantilever wing configuration. The results are presented in Figure 2, where $\eta_{strut} = 0$ is associated to the classical configuration.

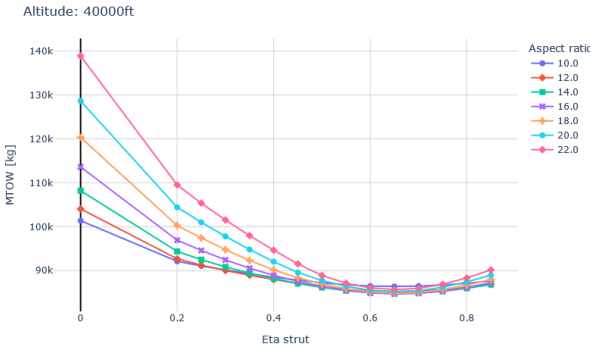


a) Evolution of the MTOW with the AR and the position of the junction

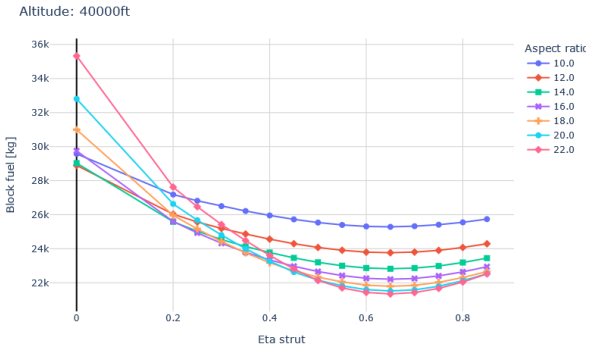


b) Evolution of the block fuel with the AR and the position of the junction

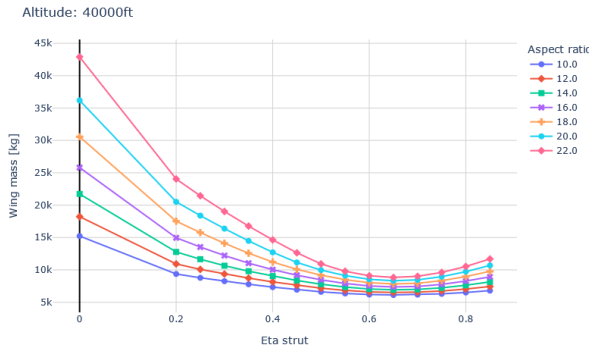


c) Evolution of the wing weight with the AR and the position of the junction

**Figure 2. Strut-Braced Wing - Influence of the AR on the SBW weight estimations.**

Compared to the cantilever configurations, the presence of the strut induces an important weight reduction. An optimized position for the junction between the strut and the wing in the spanwise direction can be identified between 60% and 65% and seems to be independent from the AR considered. Additionally, Figure 2-b indicates that the maximum weight reduction is reached for an aspect ratio between AR = 18 and AR = 20 while further increasing the AR does not lead to more weight reduction. This last statement leads to the selection of the configuration with AR = 19 for the dedicated aerodynamic optimization study presented in the following section.

## 2.4 Aerodynamic design and optimization

### *2.4.1* Impact of the wing profiles on the SBW configuration aerodynamic performances

Based on the reference ALBATROS SBW concept, the impact of the wing profiles on aerodynamic performance are assessed. CFD Euler computations are performed using the aerodynamic computational chain described in §2.1. The drag breakdown is computed for both configurations with the ONERA far-field drag extraction software *ffd* to evaluate the different physical drag components based on the Van der Vooren and Destarac formulation. In the present study as Euler simulations are considered, only the wave and induced drag components are assessed.

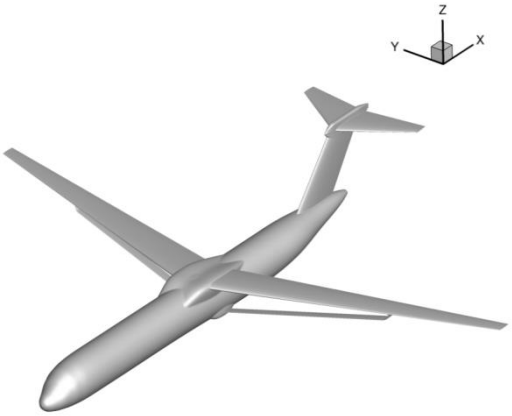


**Figure 3. Strut-Braced Wing - Geometry modelling of the reference SBW AR = 16 configuration.**

The wing profiles of both the ONERA NOVA [6] and ALBATROS [2] concepts are compared as a starting point. The latter profiles were specifically designed for transonic SBW concept but for an operating cruise Mach number of M = 0.75 hence it was decided to perform first the comparison study at this specific Mach number.

CFD computations are achieved considering the Euler equations for flow conditions representative of the cruise conditions at an altitude of 11.0 km. Target lift coefficients are directly set in the CFD solver and reached through the modification of the angle of attack. A polar evolution of the induced and wave drag coefficients is presented in Figure 4 for both SBW configurations.

The drag breakdown presented in Figure 4 indicates that the ALBATROS profiles generate less than 15 drag counts in wave drag up to $C_L$=0.7 whereas the minimum for the NOVA profiles is 34 drag counts which can be explained by the fact that the NOVA profiles were designed for a slightly higher flying Mach number but a higher sweep angle for a cantilever wing configuration.

The values of the induced drag are compared with the theoretical induced drag coefficients (purple squares) generated by an elliptical distribution of the lift over the wing ($C_{Di} = \frac{C_L^2}{\pi\lambda}$, with λ the aspect ratio of the wing). Both the ALBATROS and NOVA profiles are equivalent in terms of induced drag and slightly superior to the induced drag generated by an elliptical distribution of the lift over the wing (Oswald factor ~ 0.95 at $C_L$=0.6).

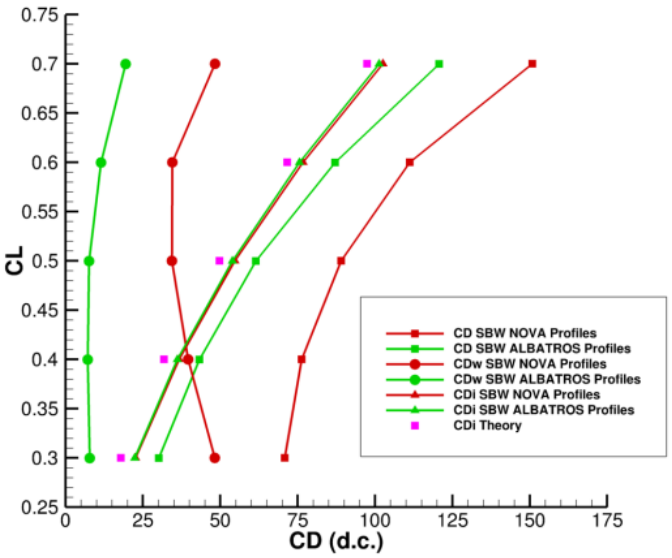


**Figure 4. Strut-Braced Wing - Drag breakdown comparison with NOVA and ALBATROS profiles on the reference SBW AR = 16 configuration.**

### *2.4.2* Optimization of the twist law of the AR = 19 SBW configuration

Based on the previous preliminary study, the ALBATROS profiles are used to model the wing of the AR = 19 configuration. The wing is parameterized by 5 control sections, illustrated in Figure 5, where the aerodynamic profiles of the wing and the strut together with the twist laws are defined as design variables of the optimization process. The objective of the optimization study is to minimize the drag generated by the strut and the wing in transonic conditions (M=0.75 and M=0.78). It was then decided to remove the horizontal tail plane which could generate some additional wave drag since it is modeled from symmetrical airfoil profiles during the optimization process. This problem is solved using on the gradient optimizer DOT MMFD of the Dakota toolbox. An illustration of the convergence process is presented in Figure 6.

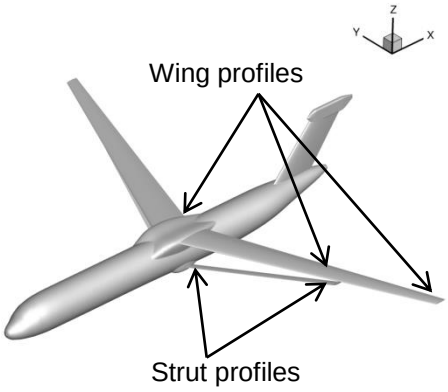


**Figure 5. Strut-Braced Wing - Identification of the wing and strut profiles on the SWB AR = 19 configuration.**

The process is considered converged after 63 evaluations at M=0.78. A comparison between the starting and the optimized twist configurations is illustrated in Figure 7 where the wave drag integration contours are displayed.

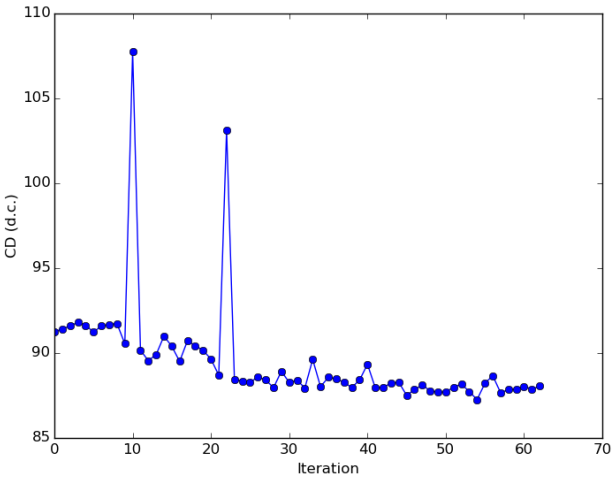


**Figure 6. Strut-Braced Wing - Convergence of the optimization process (M=0.78).**

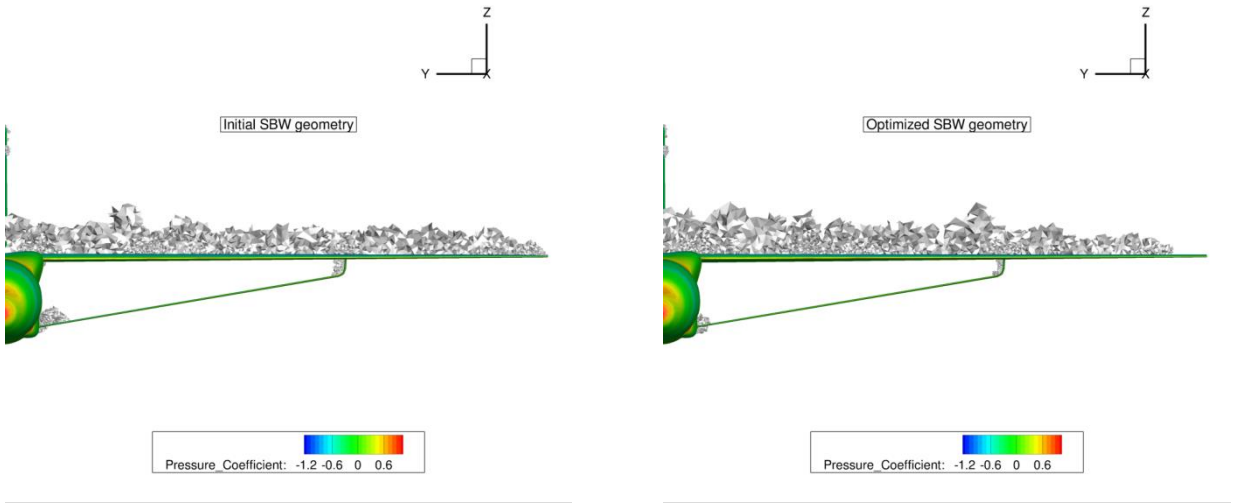


**Figure 7. Strut-Braced Wing - Comparison of wave drag integration contours after the optimization process (M=0.78).**

A slight difference appears from the comparison above, mainly at the junction between the strut and the other parts of the aircraft. More specifically at the junction between the strut and the wing, Ko et al. [19] demonstrated that the flow behaves like inside a nozzle. The modification of the twist law along the strut allowed then an increase of the area in this particular region, leading to a reduction of the wave drag generated by the geometrical junction.

The drag breakdown results are presented in Table 1 and Table 2 for the initial and the optimized SBW configurations for two Mach numbers (respectively 0.78 and 0.75). The modifications of the twist law allow reducing the wave drag by 6% and the induced drag by almost 4% for the higher Mach number. However, compared to the elliptical distribution of the lift, the Oswald factor of the optimized AR = 19 configuration is ~ 0.91. It will be interesting in the future to dedicate additional efforts to further decrease the induced drag generated by the SBW configuration by increasing the number of design variables.

For the lower Mach Number (M=0.75 - Table 2), with the optimization the wave drag component is reduced by 19% and the induced drag by 2%.

| Influence of the twist law at M = 0.78 and $C_L$ = 0.6 | | | | |
|---|---|---|---|---|
| | | Initial AR = 19 SBW configuration | Optimized AR = 19 SBW configuration | |
| | Angle of attack | 1.037 | -0.041 | |
| Drag counts | Wave drag | 22.2 | 20.76 | -6.5 % |
| | Induced drag | 69.05 | 66.5 | -3.7 % |
| | Far-Field drag | 91.24 | 87.26 | -4.4 % |

**Table 1. Strut-Braced Wing - Drag breakdown comparison between initial and optimized SBW configurations (M=0.78).**

| Influence of the twist law at M = 0.75 and $C_L$ = 0.6 | | | | |
|---|---|---|---|---|
| | | Initial AR = 19 SBW configuration | Optimized AR = 19 SBW configuration | |
| | Angle of attack | 0.9 | 0.319 | |
| Drag counts | Wave drag | 6.81 | 5.52 | 19.0% |
| | Induced drag | 66.81 | 65.57 | -1.9% |
| | Far-Field drag | 73.63 | 71.19 | -3.3% |

**Table 2. Strut-Braced Wing - Drag breakdown comparison between initial and optimized SBW configurations (M=0.75).**

This preliminary study showed that the ALBATROS profiles are still suited for higher Mach numbers even if the aerodynamic performances are slightly degraded. In the future studies, the sweep angle of the wing (and the strut) will be included in the design variables as well as the characteristics of the wing profiles (especially the camber laws) to further improve the aerodynamic performance. Moreover multiple flight point optimizations will be considered.

## 3. The BWB concept

In the frame of the Clean Sky 2 AIRFRAME ITD platform [10], ONERA made important efforts to design a SMR BWB concept family without and with BLI engine integration. Based on the same tool suite as for the HAR SBW concept, the SMILE (Small - Medium range Integrated Light and Efficient aircraft) configuration has been designed and optimized in order to maximize the lift-to-drag ratio in cruise conditions [8] while taking into account internal volume and handling quality constraints.

### 3.1 Methodology

#### *3.1.1* Previous work

The current work is based on a multi-disciplinary optimization (MDO) of a short-medium range BWB carried out at ONERA in the frame of Clean Sky 2 [9][10]. This MDO uses an Overall Aircraft Design (OAD) process developed since 2015 at ONERA [21]. Six disciplinary modules are part of this process: Aircraft Geometry, Propulsion, Aerodynamics, Structure & Weight, Mission & Performance and Handling Qualities. A description of the low-fidelity Aerodynamics Module is given in [22].

The top-level aircraft requirements (TLAR) considered for these design activities are the following:

- Payload of 150 pax with 90 kg per pax
- Range of 5100 km
- Mach 0.78

The process allows exploring a great variety of BWB planforms. A MDO problem is defined with the objective to minimize the mission fuel weight, the main constraints being the take-off distance, the climb duration and the handling qualities. The resulting configuration has been named SMILE (Small - Medium range Integrated Light and Efficient aircraft). Its planform constitutes the starting point of the work presented here after. The OAD process also gives the size and arrangement of the pressurized zone.

The objective of this work is hence to obtain an efficient 3D aerodynamic shape, keeping the planform given by the MDO. Engine integration is first not taken into account, as the objective is first to get an efficient glider shape.

### *3.1.2* Optimization Chain

This work uses the same computational tool chain as described in §2.1. An optimizer is coupled to this automatic process, in order to be able to solve the optimization problem (see Figure 8). The choice was to use the Dakota Toolbox and the gradient based optimizer DOT MMFD (Modified Method of Feasible Directions) [23]. A gradient-free optimizer is more capable of finding the best minimum in a case of a problem with multiple local minima. However, the high number of function calls made the use of this type of optimizer convergence of gradient based methods are the main motivation behind their usage, especially when they are combined with heavy CFD codes.

Even if the SU2 and elsA codes have an ajdoint capability, the adjoint information is not fully propagated yet through the mesh and CAD processes. In this case, gradient values were then obtained via finite difference computations. The optimization chain can solve either the Euler flow equations or the RANS ones, at the only cost of computer load increase.

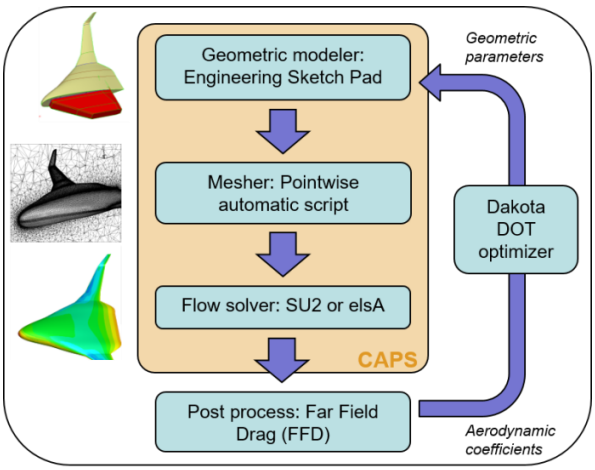


**Figure 8. Blended Wing Body - Overview of the optimization chain.**

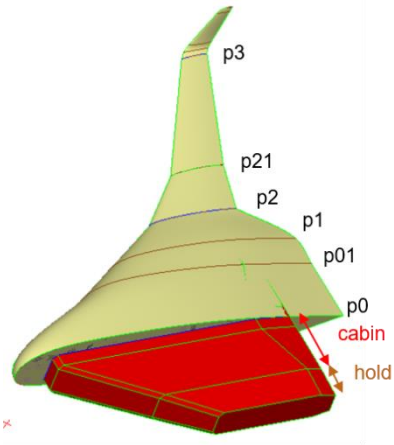


**Figure 9. Blended Wing Body - BWB half geometry (in beige) and half geometry of the pressurized volume (in red) [10].**

## 3.2 Glider optimization

In order to obtain an efficient form, the BWB geometry has been parameterized, to allow its modification and its complete definition by a finite set of parameters. As seen in Figure 9, the BWB is defined using six sections. The choice was made to parameterize the airfoils using the Class Shape Transform (CST) parameterization [19]. This method uses Bernstein polynomials weighted by a shape function to define completely the upper and lower side of the airfoil. Because of the use of finite differentiation and to limit the computational cost, each airfoil is parameterized using only eight CST coefficients (four on each side). The other parameters not fixed by the planform are the twist angles on each section. Finally, the winglet geometry is kept fixed, its shape being defined by lofting the last airfoil “p3” (see Figure 9). The angle of attack is also left free to respect the lift coefficient constraint.

In total, the optimization problem can use 55 design variables to modify the aircraft shape:

- 6*8 = 48 for the airfoils shapes
- 6 twist angles
- 1 angle of attack

The main geometric constraint is represented in Figure 9 by the internal pressurized volume in red. The dimension of this volume has been fixed by the OAD process taking into account the cabin layout. Some margins have been added to account for the aircraft structure, allowing using this volume directly as a geometric constraint. ESP allows computing the intersectional volume between the exterior shape and the internal one. This value is then extracted to constrain the optimization process. On the outer wing section, only a minimum relative thickness constraint on the three design sections is used. As the number of design variables is quite important and since finite differences are used for the evaluation of the sensitivities, three optimizations have been run successively, optimizing only subsets of the design variables at each step.

The optimization aiming at improving the aerodynamic efficiency, the objective is naturally to minimize the aircraft drag coefficient ($C_D$), while maintaining a sufficient lift level. In this case, as the OAD process gives the aircraft mass balance and reference surface, it fixes the cruise lift coefficient ($C_L$) at a value of 0.273. The same process also fixes the cruise aerodynamic conditions. In addition to the lift constraint, as a BWB aircraft does not have any tail stabilizer, a trim constraint is thus added. To respect this trim condition, at the targeted lift value, the longitudinal moment coefficient computed at the center of gravity ($Cm_{cog}$) should be zero. This ensures that the center of pressure coincides with the center of gravity, implying that the aircraft is trimmed during cruise, without the need to deflect any control surface, which would cause a drag penalty.

As highlighted in previous works [24][25], the challenge posed by the BWB configuration manly lies in the central body. The need for a moderate angle of attack is implemented in the optimization problem by bounding the angle of attack variable. Only the cruise conditions were considered (single point optimization). A low-speed evaluation of the current design should be added to the presented work, notably to check the take-off rotation criteria, as mentioned in [26].

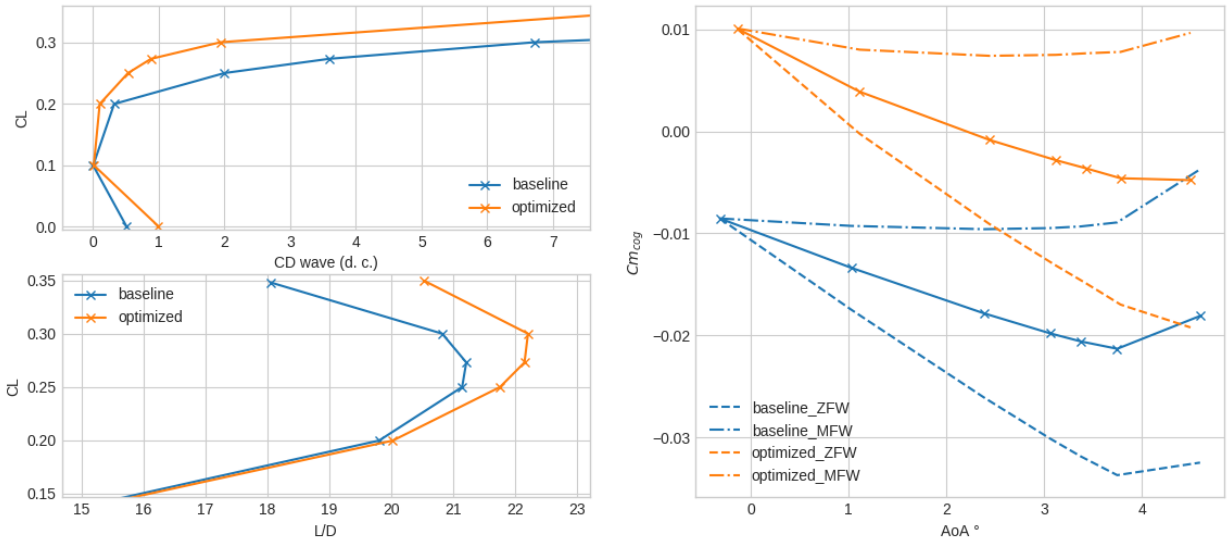


**Figure 10. Blended Wing Body - Comparison of the baseline and optimized geometries, using RANS computations.**

Figure 10 presents the polar comparison of the resulting optimized configuration compared to the baseline, evaluated with RANS computations. The bottom panel of Figure 10 shows the moment coefficient computed for three different positions of the center of gravity. Slopes of these curves remain negative, meaning a positive static margin, which ensures a stable aircraft. It can be seen that the trim condition is not totally satisfied for the mean position of the center of gravity (solid line), the moment coefficient having a slight negative value. Further optimizations have been performed to improve this point, but they have only been realized at the price

of worst L/D ratio or higher cruise angle of attack. Since the trim condition varies quite a lot with the variation of the aircraft weight during cruise, which induces a displacement of the center of gravity by approximatively one meter, the obtained configuration was dubbed satisfying.

On the top panel of Figure 10, it can be seen that the wave drag has been reduced by two drag counts at the cruise lift coefficient. This can also be seen in Figure 11, where high-pressure zones are reduced on the outer wing of the optimized design. Figure 12 shows a reduced pressure peak on the outer wing (y/b = 0.8), compared to the baseline geometry.

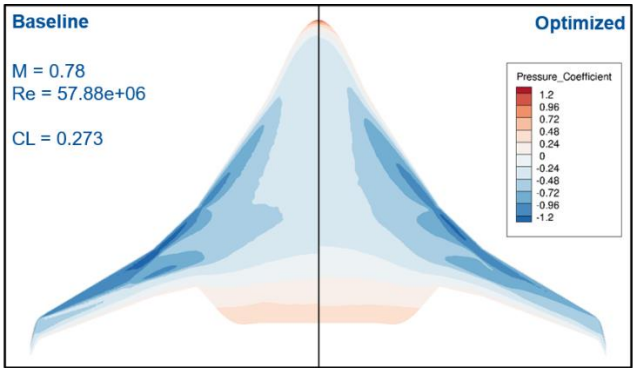


**Figure 11. Blended Wing Body - Pressure coefficient comparison on the baseline and optimized configurations.**

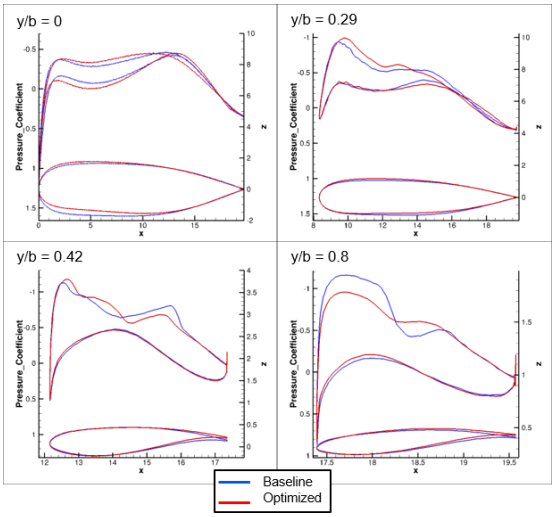


**Figure 12. Blended Wing Body - Comparison of pressure coefficients and airfoils on four spanwise locations of the baseline and optimized configurations.**

## 3.3 BLI design

The parametric modeler ESP allows exploring a great variety of design, when dealing with engine integration. The concept considered here is to integrate a high by pass ratio turbo-fan on the top of the BWB aircraft. In this position, the engines are supposed to ingest a part of the boundary layer that develops on the upper side of the inner body. Boundary layer ingestion (BLI) has the capacity to provide additional fuel burn reduction compared to conventional engine installation. This was demonstrated experimentally and numerically by Carrier et al. in [5]. In a BWB context, Kawai et al. [27] have shown a potential fuel burn reduction between 5 to 10 percent. Literature on BLI installation on a BWB is quite scarce, the main works having been done by NASA and Boeing in the early 2000s, including wind tunnel testing [28]. BLI allows re-energizing the fuselage boundary layers, improving the overall energy balance of the aircraft. Additional benefits lay in the reduction of the nacelle wet surface and a weight reduction due to the absence of pylons compared to a podded integration. In the current case, the fact that a small BWB aircraft is considered, geometric constrains (mainly the internal pressurized volume) are even more pregnant than on a long range BWB.

To obtain the results presented here after, the same computational chain presented in §2.1 was used. Engines are modelled by using inlet boundary conditions, specifying density and velocity vector at the inlet and outlet of the engine. These values are obtained by using a simple thermodynamic model of a double flux turbo-fan, considering a fan pressure ratio of 1.3, representative of a modern Ultra High ByPass Ratio engine. Thrust is estimated to equilibrate the drag of a complete aircraft with an estimated L/D of 20.5. With this value, the thermodynamic model gives the fan diameter, the pressures and mass flows, with the hypothesis of an adapted nozzle. RANS computations are conducted, with the Spallart-Allmaras turbulence model. The boundary conditions used do not allow to fully account for BLI benefits (the boundary layer is lost inside the engine block). In future work, the body force methodology will be used to model the engine, in order to precisely quantify the

effect of the BLI on the configuration. However, the current setup allows quickly spotting detached zones mainly at the inlet, the nacelle sides, and the trailing edge junction. Concerning the inlet, an S-duct shape has been employed to realize the junction between the BWB upper side and the fan face.

On the trailing edge junction, a large separation bubble can appear if the engine nozzle is significantly higher than the BWB trailing edge. This was particularly highlighted by Kim and Liou in [29] (Figure 13). This detached zone increases the overall pressure drag, and should be avoided.

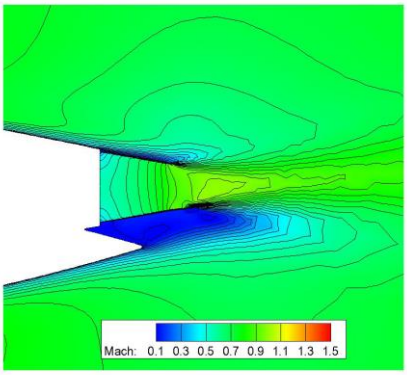


**Figure 13. Blended Wing Body - Separation bubble which can appear on the trailing edge region, from [28].**

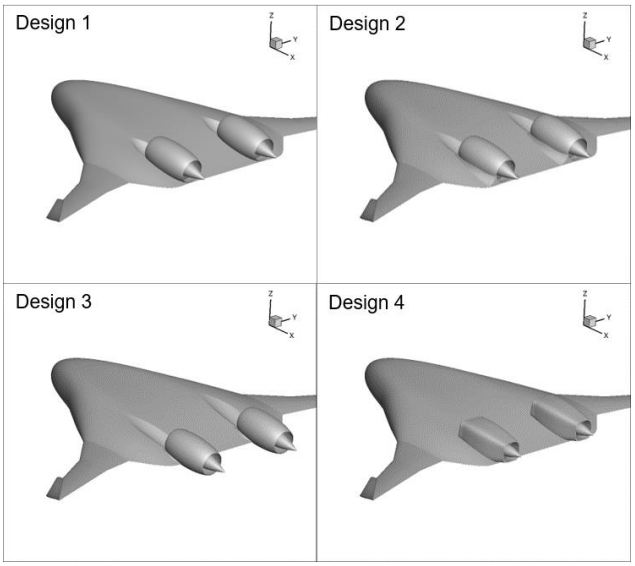


**Figure 14. Blended Wing Body - Overview of four different engine integration designs.**

Figure 14 presents four different designs On Designs 1 and 2, the trailing edge issue has been taken into account, and the engine is positioned so that the nozzle coincides with the BWB trailing edge. Due to the simplified capabilities of ESP, Designs 1, 2 and 3 are modelled by making an union between a circular nacelle and the BWB body. An S-shape tube is then subtracted from the geometry to realize the S-duct entrance. Design 4 is a try to use a non-circular nacelle, which could prevent detached areas appearing on the acute side angles formed between the nacelle and the upper side of the BWB.

Figure 15 shows the Mach field in a spanwise slice containing the fan. A detached area in the S-duct appears in Design 1. Design 2 solves this issue, with a much longer S-duct. It must be stressed that the S-duct of these two designs intersects the internal pressurized volume considered in Figure 9, which violates the geometry constraint. Complying with this constraint, imply to reduce the S-duct length. Then, there is only two solutions to prevent from an abrupt slope: either move the engine upward (which would create the trailing edge issue of Figure 13) or move the engine backward. The last solution is retained in Design 3.

Figure 15 highlights that great care should be taken when designing the side junction between the nacelle and the wing. It is particularly visible that big corner separation flows are developing in these regions. Design 2 tries to solve this issue by adding fillet junction compared to Design 1. It effectively suppresses the detached zone on the external side. Because Design 3 moves the engines to the rear, the length of the acute angle is reduced, and a small fillet can effectively suppress the separated areas. Thus, Design 3 presents several advantages compared to the two others, regarding the aerodynamic performance. However, it must be stressed that the structural integration of this design appears unfavorable (see Figure 15 bottom), compared to Designs 1 and 2. In the fourth configuration (Design 4), the limited capabilities of ESP (limited control of the nacelle profile), prevents from the definition of a precise enough geometry. Then, the geometry evaluated presents several detached zones around the nacelle, and the S-duct slope is too steep to keep the flow attached upstream of the fan face.

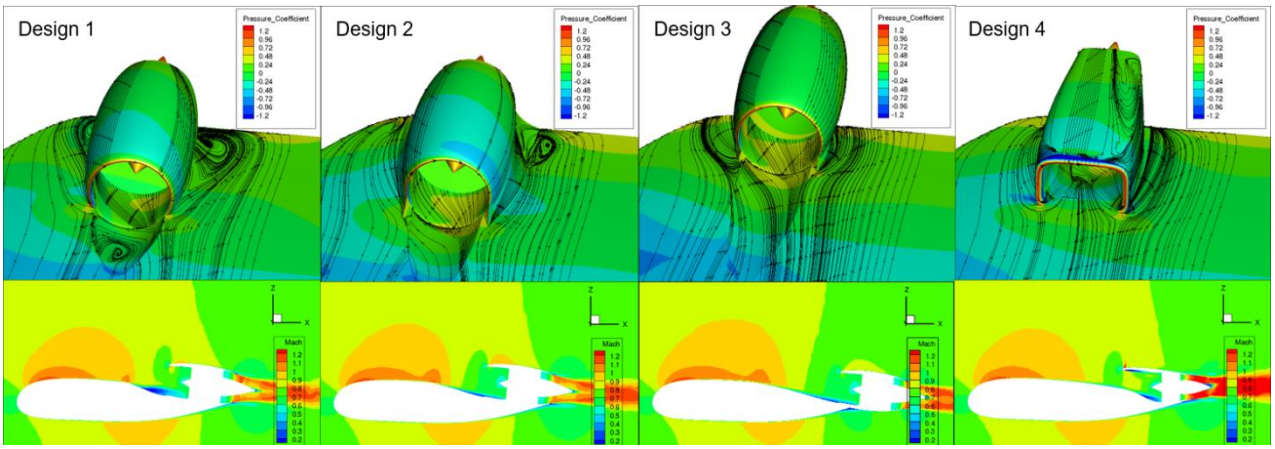


**Figure 15. Blended Wing Body - Upper part: Surface pressure coefficient and friction vectors around the engine. Lower part: Mach field in the y-plane slice containing the fan.**

As the aim of this study is to assess the potential gains of BLI engine installation on a BWB, Design 3 has been retained so far. The body force methodology associated with exergy balance is currently being employed to account the potential gains of the BLI on this configuration.

# 4. Distributed Propulsion

## 4.1 The choice of ducted fans

When dealing with distributed propulsion, either propellers or embedded fans can be considered. Distributed propellers will be suitable up to a cruise Mach number of 0.6-0.7 approximately. Beyond (up to M=0.70-0.75), high speed propellers must be used, which requires more power. For Mach numbers larger than 0.75, ducted fans become necessary (because the inlet will slow down the Mach number to 0.6-0.65 in the fan plane, for which the fan efficiency is the best). Flying at such Mach number requires a Fan Pressure Ratio value of FPR=1.30, a small value compared to modern turbofans, but much larger than for propellers.

In the frame of the Clean Sky 2 Large Passenger Aircraft (LPA) platform, ONERA has explored the possible implementation of Hybrid Electric Distributed Propulsion on a transport aircraft carrying 150 passengers at a cruise Mach number of 0.78 over a range of 1200 NM to match airlines flexibility requirements. Consequently, the choice of ducted fans was mandatory. To perform conceptual design studies, a research baseline concept called DRAGON (Distributed fans Research Aircraft with electric Generators by ONERA - see Figure 16) has been defined, characterized by distributed fans located all along the wing span on the pressure side in a rearward position, this configuration has been investigated by disciplinary experts ([8][12]). Regarding aerodynamics, a dedicated 3D process of a representative wing section has been set-up in order to design a first configuration with a proper aerodynamic behavior. This exercise is quite complex as many constraints have to be fulfilled and the sweep angle of the wing makes the design of the nozzle particularly challenging (see Figure 17).

## 4.2 Position of the ducted fans

When designing the aerodynamic of the Hybrid Electric Distributed Propulsion (HEDP), the work of Wick [30] was a valuable reference because it studies many engine positions on the airfoil. After a detailed review of the results, one promising option for high speed cruise Mach number features the engine on the pressure-side of the airfoil (Figure 16). Indeed, the key issue at high speeds is that the upper wing in transonic condition contains a supersonic area which is very sensitive to any obstacle (an upper engine configuration could trigger buffet onset for example). Therefore the suction side must remain as clean as possible. Furthermore, the pressure side naturally helps to slow down the flow upstream of the engine inlet. Consequently, the pressure side-rearward position has been selected by the DRAGON team as the starting point of the aerodynamic design.

**Figure 16. Distributed Propulsion - Illustration of the DRAGON concept [8].**

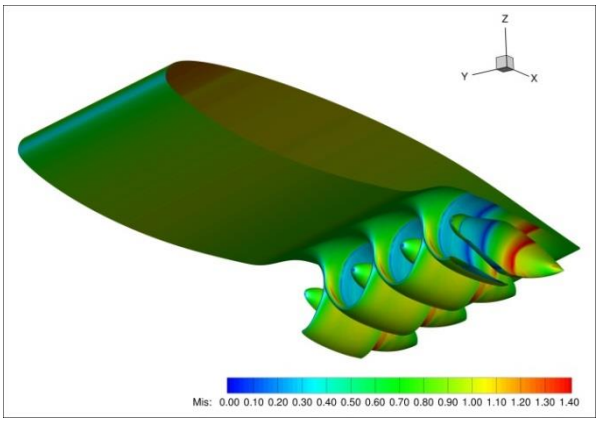


**Figure 17. Distributed Propulsion - Example of aerodynamic configuration obtained during the design procedure.**

The design process was split in two parts:

- first, some design iterations on a 2.5D configuration;
- then, further design on a periodic 3D configuration, including the wing sweep angle.

## 4.3 2.5D design of a multi-fan Distributed Propulsion

The first step of the design consisted in finding the best position of the engine chordwise. In order to iterate fast, the design was performed in 2.5D, meaning a 2D airfoil with a 25° sweep angle. This assumption allows computing the configuration at the real Mach number, but the engine section is then infinitely long and rectangular. Because the nozzle is chocked at cruise, the nozzle throat controls the mass flow rate. As the nozzle throat in 2.5D is not the one of a circular nozzle, the 2.5D method is fast and efficient, but inaccurate to get a true distributed fan design that requires a 3D design presented hereafter.

The coupling between the engine and the airfoil in transonic conditions is strong. Therefore an easy but unrealistic reference starting point was chosen, placing the engine at the end of the airfoil trailing edge, thus giving a smooth flow everywhere, and preventing having a diverging nozzle (Figure 18, more details can be found in [8]). Moving the engine forward, the iterative design process led to a good compromise, which was then converted into a 3D design.

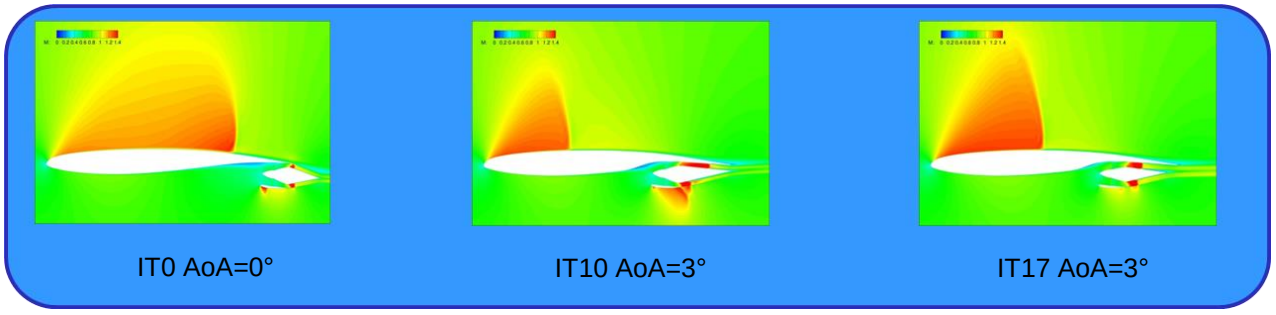


**Figure 18. Distributed Propulsion - Some aerodynamic iterations based on 2.5D design. Ideal engine position (left), intermediate iteration for realistic engine position (centre), final 2.5D status (left). All computations are at M=0.80, 35000 ft.**

## 4.4 3D design of the multi-fan Distributed Propulsion

The main challenge when designing a 3D integration of distributed fans with sweep angle is to ensure a periodicity between each engine, without compromising the necessity to design smooth aerodynamic surfaces. A “periodic design method” was thus created, where only one engine is designed, but split in two halves. The

split is in the symmetry plane of the engine (Figure 19). More details and comparison between 2.5D and 3D results are available in [12].

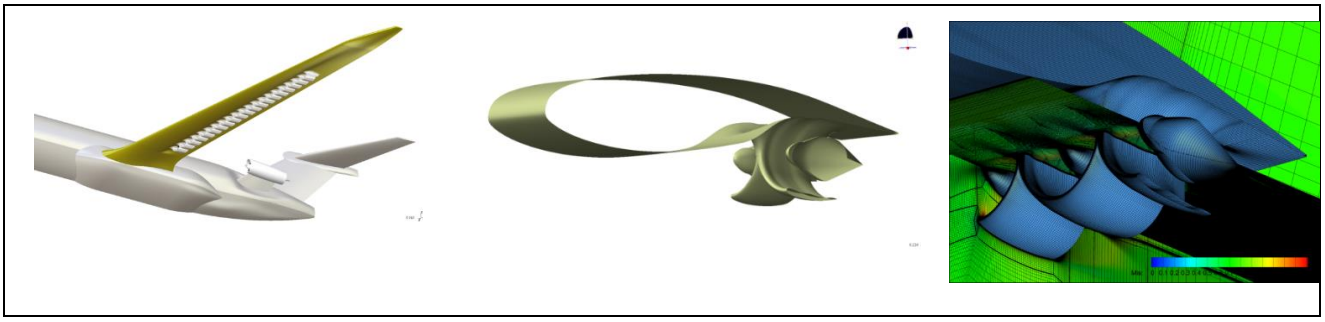

**Figure 19. Distributed Propulsion - "Periodic design method": one engine is designed, split in two halves (center), to ensure geometric periodicity on a wing with sweep angle (left). Example of structured mesh on the right.**

Another challenge is to design a transition from a 2D airfoil to a cylindrical section before the inlet, and then to come back to a 2D airfoil after the nozzle, within a very short length. The streamtube coming through the engine is rectangular before the inlet, then circular into the engine, and finally rectangular again after the nozzle. As boundary layers are very sensitive to corners and pressure gradients, a major stake is to find shapes that do not trigger flow separations. Before the inlet, the flow faces a negative pressure gradient, in order to slow down the velocity from transonic speeds to approximately M=0.65 in the fan plane. Furthermore, part of the streamtube is the boundary layer of the airfoil, so that it must sustain the compression as in a Boundary Layer Ingestion (BLI) configuration. After the nozzle, the flow must expand to supersonic speeds (chocked nozzle), but one part of the flow is constrained by the airfoil rear part (making a diverging cross section), which makes the flow accelerate too much if the design is not correctly managed. Those challenges are addressed thereafter, using an iterative manual design process.

3D computations were performed using elsA [16] (Airbus-Safran-ONERA property) in steady RANS with the Spalart-Almaras turbulence model at M=0.80, 35000 ft, AoA=2°. The fan was modeled using an actuator disk with a uniform pressure jump of dP=5000 Pa (corresponding to FPR=1.13), 8000 Pa (FPR=1.20) and 10900 Pa (FPR=1.30).

### *4.4.1* First iterations: improving the design of the intake lips

The last 2.5D configuration (IT17) was converted to a 3D design named G17 (Figure 20). As expected, that design features many issues: leading edge overspeeds and flow separations, nozzle flow separation, and large nozzle Mach number. However, no flow separation appears before the inlet on the airfoil side, which is very positive.

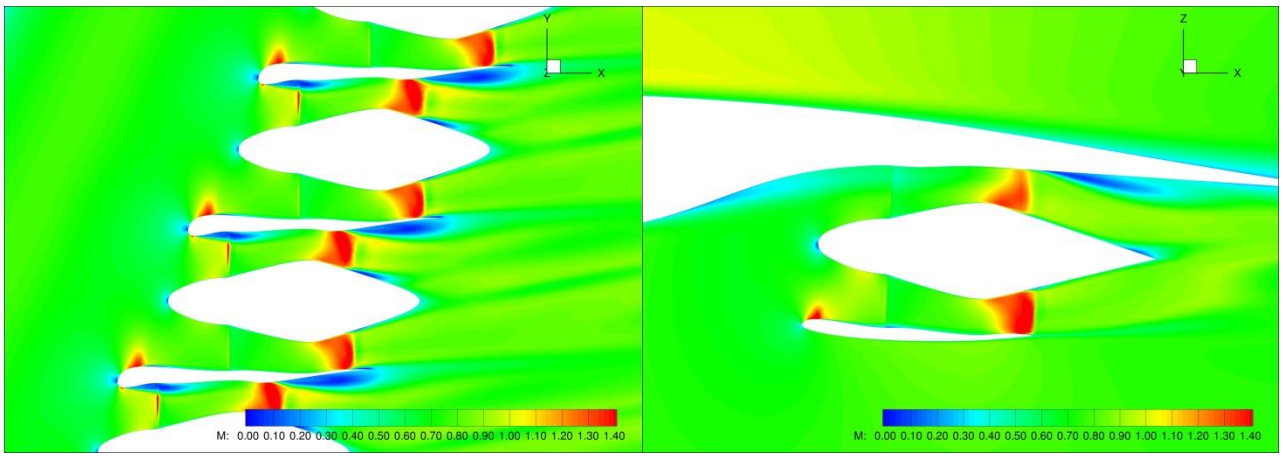


**Figure 20. Distributed Propulsion - First 3D configuration named G17 - M=0.80 AoA=2°, FPR=1.13.**

### *4.4.2* Changing the nozzle plug shape

After some manual iterations, configuration G19-61 shows fewer issues (Figure 21). A large flow separation remains on the nozzle cone (named plug hereafter), but at the targeted FPR=1.30 only. Previously, the nozzle throat section was too small to reach the targeted FPR. Main design improvements are a smooth inlet lip (no more supersonic areas), a modified nozzle throat, and a modified plug shape. Instead being axisymmetric, it is now coming upward, close to the airfoil lower surface. The purpose of that modification is to reduce the diverging section between the plug and the airfoil surface, hoping it helps lowering the acceleration in that area.

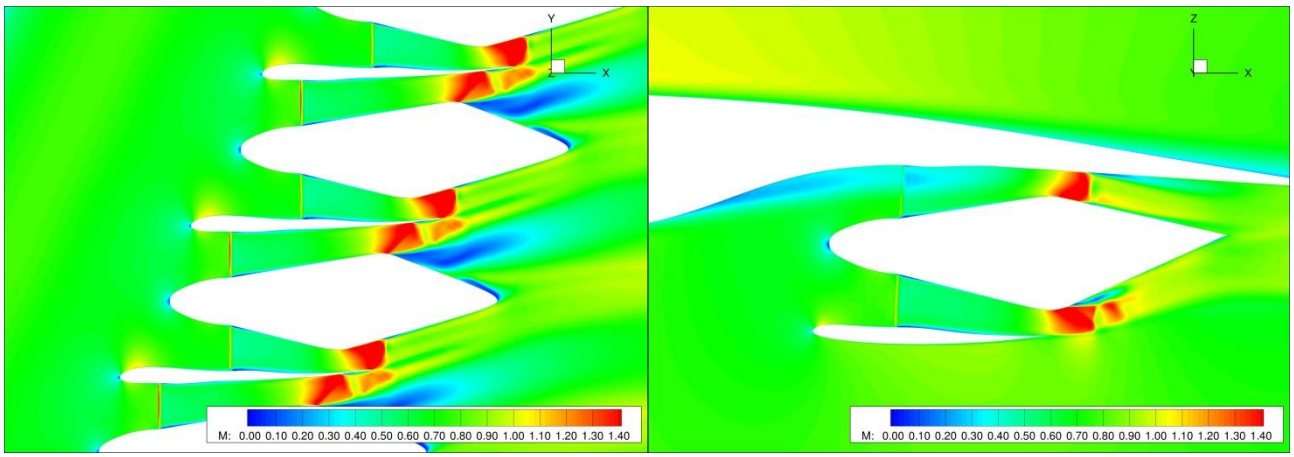


**Figure 21. Distributed Propulsion - Configuration G19-61 - M=0.80 AoA=2°, FPR=1.3.**

Additional iterations on the G19-6x series led to the G19-72 (Figure 22). Differences with G19-61 are smaller, but helps in cancelling the flow separations in the symmetry plane. The main idea it to shift the plug ending laterally. Therefore, the plug shape follows the sweep angle of the wing. However, it was not enough, as a large separation remains on the side of the plug.

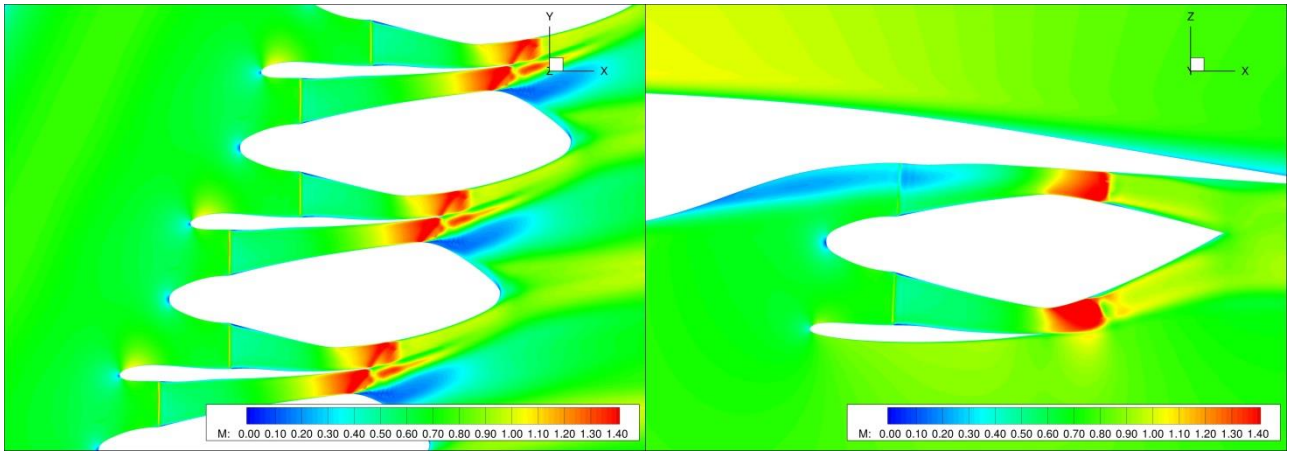


**Figure 22. Distributed Propulsion - Configuration G19-72 - M=0.80 AoA=2°, FPR=1.3.**

In order to get a theoretical target of the configuration, some Euler computations were performed in order to remove flow separations. For example, Figure 23 displays G19-81 in Euler, whereas Figure 24 is in RANS. In the Euler case, the nozzle chocked region is at angle, as wished. Desperately, the diverging section in the nozzle amplifies the Mach number beyond acceptable levels, thus triggering to flow separations when switching to RANS (Figure 24).

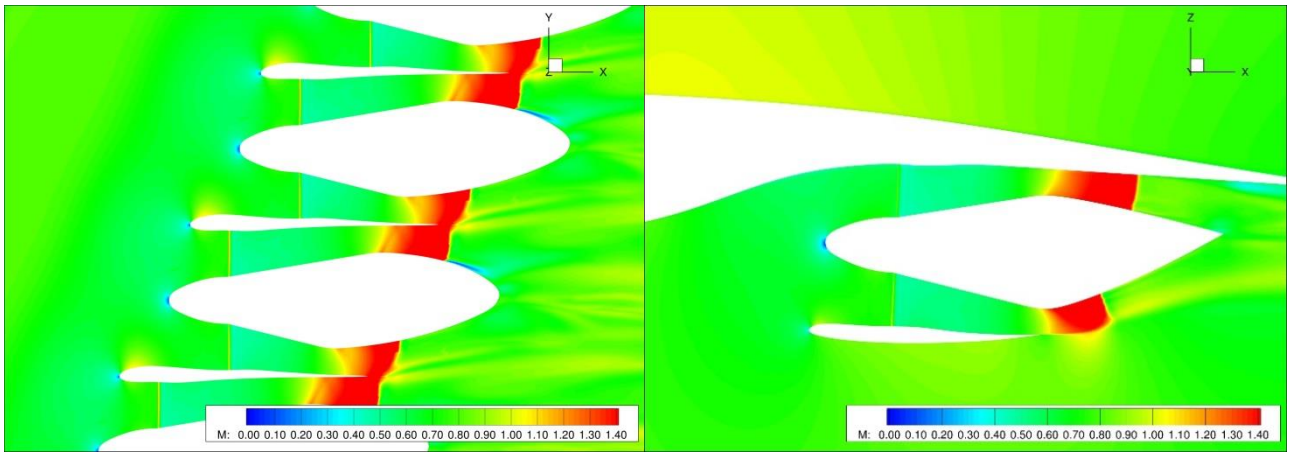


**Figure 23. Distributed Propulsion - Configuration G19-72 – M=0.80 AoA=2° in EULER, FPR=1.3.**

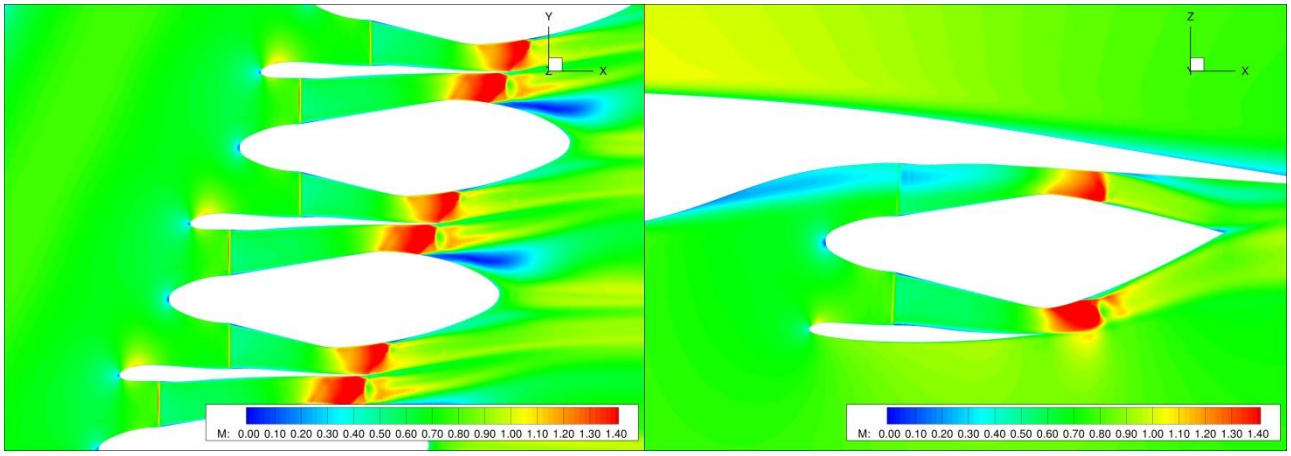


**Figure 24. Distributed Propulsion - Configuration G19-72 - M=0.80 AoA=2° in RANS, FPR=1.3.**

### *4.4.3* Lengthening the nozzle plug

After many iterations on the G19-8x series, an improvement came from the G19-9x series. The G19-93 as a much longer but smoother plug shape (Figure 25). There is no more small curvature radii on the shape, which is helpful to dampen the diverging section in the nozzle. Figure 25 shows Euler computation at a smaller FPR=1.13), and highlights that the flow is improved, though still far from the target.

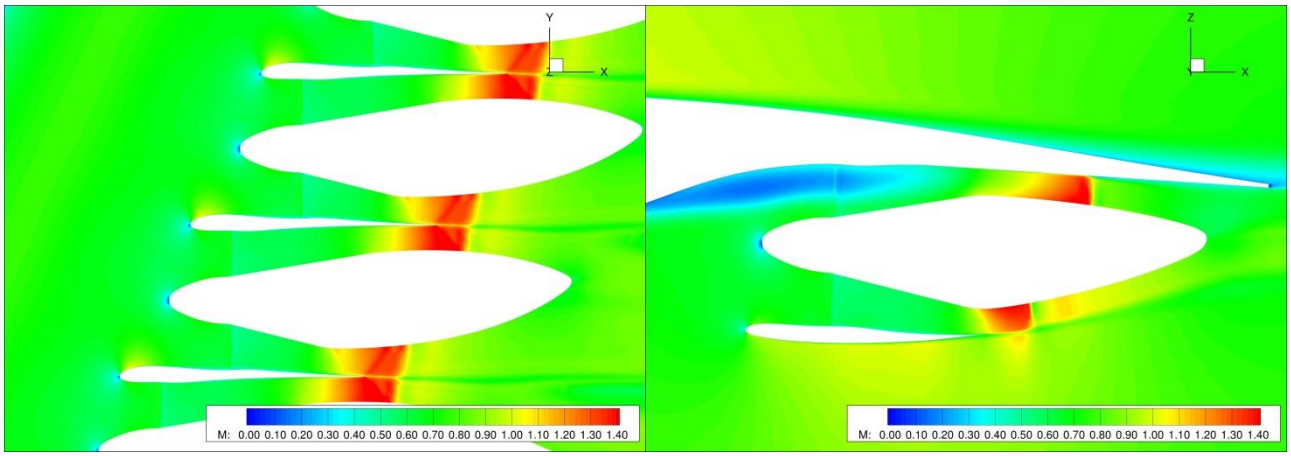


**Figure 25. Distributed Propulsion - Configuration G19-93 - M=0.80 AoA=2° in EULER, FPR=1.13.**

When comparing G19-93 in RANS (Figure 26), FPR=1.30, to G19-72 (Figure 22), the modifications of the

nozzle plug and their impact on the flow are more obvious.

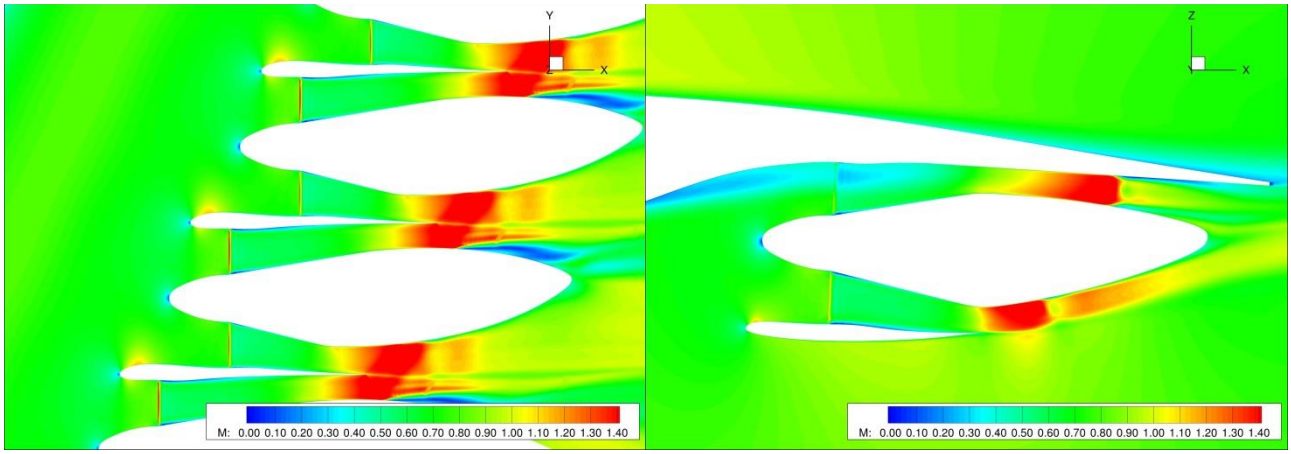


**Figure 26. Distributed Propulsion - Configuration G19-93 - M=0.80 AoA=2° in RANS, FPR=1.30.**

The iterative design process had to be stopped due to the project constraints, without finding a complete satisfying solution for M=0.80, FPR=1.30. However, the last G19-101 configuration was computed at a lower FPR=1.13, showing a very proper aerodynamic behaviour (Figure 27).

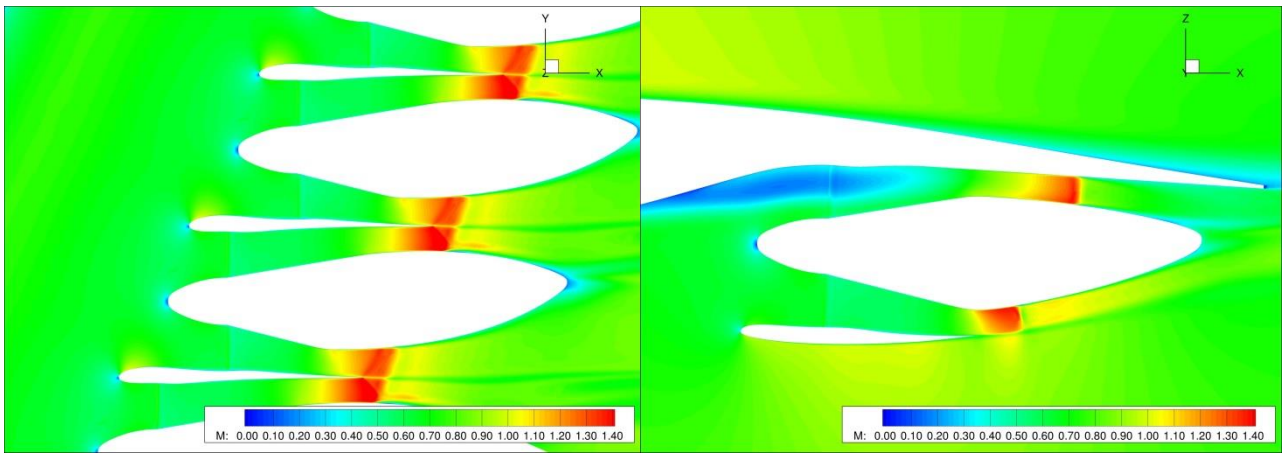


**Figure 27. Distributed Propulsion - Configuration G19-101 - M=0.80 AoA=2° in RANS , FPR=1.13.**

### *4.4.4* Transonic distributed propulsion: lessons learned

The ambitious target to design a 3D detailed configuration of distributed propulsion was satisfied. As expected, the nozzle design was the most difficult part. However, the intake part was much easier than anticipated.

As far as the nozzle is concerned, having the nozzle plug outside of the nacelle shape can creates a large diverging cross section in cruise conditions. A possible way of improvement is to design a longer nacelle fairing, so that the plug remains inside the nacelle shape which was partially done in the results presented before. Nevertheless, this solution adds wetted area and so drag. In order to find the best compromise at aircraft level between the length of the plug and the propulsion efficiency additional analysis are needed. For that purpose, far-Field exergy-based decomposition using the in-house *ffx* code are on-going on the last configuration (G19-101).

## 5. Conclusions

An overview of aerodynamic design activities performed on innovative aircraft concept in the frame of the Clean Sky 2 Programme is proposed in this paper. Three configurations corresponding to three EIS targets

are presented: Strut-Braced Wing, Blended Wing Body and Distributed Propulsion concepts dedicated to a SMR-like mission.

For the SBW concept, a detailed aerodynamic design of the configuration with an Aspect Ratio of 19 (best aero-structural compromise at aircraft level) has been achieved using an automatic shape optimization process. A relevant first configuration minimizing the induced and wave drag components has been obtained. Additional optimizations with more design variables are currently conducted to further improve the aerodynamic performance of the AR19 SBW ONERA concept.

For the BWB configuration, a family concept is proposed: first a glider configuration has been designed in transonic cruise conditions achieving very high Lift-to-Drag ratio (around 21), then a derivative concept with BLI engine integration is proposed and is currently under investigation to have an accurate evaluation of the BLI benefits using advanced post-processing methods. A third concept will be proposed soon in the frame of the H2020 IMOTHEP project coordinated by ONERA with distributed propulsion and ducted fans.

The last concept is the DRAGON hybrid-electric configuration proposed by ONERA. In this paper, the detailed aerodynamic design performed on a 3D CAD model is described underlying the engine integration challenge when considering the Distributed Propulsion technology on a cantilever wing in transonic conditions. A first shape with a proper aerodynamic behavior has been obtained and additional analysis are on-going the identify the physical origin of the aerodynamic benefits with such a configuration.

## 6. Acknowledgment

The work presented in this paper on the SBW concept has been funded by the European Union through the CleanSky2 project U-HARWARD, under grant Grant agreement ID: 886552. The work on the BWB configuration has received funding from the Clean Sky 2 Joint Undertaking under the European Union's Horizon 2020 research and innovation program under grant agreement N°CS2-AIR-GAM-2020-2021-01. The work on the DP concept has received funding from the Clean Sky 2 Joint Undertaking under the European Union's Horizon 2020 research and innovation program under grant agreement N°CS2-LPA-GAM-2018-2019-01.

The authors would like also to thank ONERA colleagues for their contributions to OAD and aerodynamic design activities (J. Gauvrit-Ledogar, S. Defoort, C. David and G. Carrier).

## 7. References

[1] https://op.europa.eu/fr/publication-detail/-/publication/296a9bd7-fef9-4ae8-82c4-a21ff48be673

[2] G. Carrier and al. "Investigation Of A Strut-Braced Wing Configuration For Future Commercial Transport". ICAS 2012.

[3] G. Carrier and al. "Multidisciplinary analysis and design of strut-braced wing concept for medium range aircraft". AIAA Scitech January 2022. 10.2514/6.2022-0726.

[4] Liebeck, R. H. (2004). Design of the blended wing body subsonic transport. Journal of aircraft, 41(1), 10-25.

[5] G. Carrier and al. "Numerical and Experimental Aerodynamic Investigations of Boundary Layer Ingestion for Improving Propulsion Efficiency of Future Air Transport", AIAA paper 2013, https://doi.org/10.2514/6.2013-2406

[6] Wiart L., Atinault O., Paluch B., Hue D. and Grenon R. Development of NOVA Aircraft Configurations for Large Engine Integration Studies, 33rd AIAA Applied Aerodynamics Conference, June 22-26, 2015, Dallas, TX.

[7] M. Iwanizki and al. "CONCEPTUAL DESIGN STUDIES OF UNCONVENTIONAL CONFIGURATIONS", Aerospace Europe Conference 2020, 25-28 February 2020, Bordeaux, France.

[8] Q. Bennehard, 'AERODYNAMIC SHAPE OPTIMIZATION OF A SHORT MEDIUM RANGE BLENDED WING BODY AIRCRAFT', 56th 3AF International Conference on Applied Aerodynamics, 28 - 30 March 2022, Toulouse – France.

[9] J. Gauvrit-Ledogar, et al. "Multidisciplinary Design and Optimization of the Blended Wing Body Configuration SMILE", 9TH EUROPEAN CONFERENCE FOR AERONAUTICS AND

SPACE SCIENCES (EUCASS), July 2022, Lille, France.

[10] J. Gauvrit-Ledogar and al., 'MULTIDISCIPLINARY DESIGN ANALYSIS AND OPTIMIZATION PROCESS DEDICATED TO BLENDED WING BODY CONFIGURATIONS', 33rd Congress of The International Council of the Aeronautical Sciences (ICAS), September 4th – 9th, 2022, Stockholm, France.

[11] P. Schmollgruber and al. "Multidisciplinary Exploration of DRAGON: an ONERA Hybrid Electric Distributed Propulsion Concept, AIAA paper 2019, https://doi.org/10.2514/6.2019-1585

[12] P. Schmollgruber and al. "Multidisciplinary design and performance of the ONERA Hybrid Electric Distributed Propulsion concept (DRAGON)", AIAA paper 2020, https://doi.org/10.2514/6.2020-0501

[13] Haimes, Robert, et al. "Multi-fidelity geometry-centric multi-disciplinary analysis for design." AIAA Modeling and Simulation Technologies Conference. 2016.

[14] Haimes, Robert, and John Dannenhoffer. "The engineering sketch pad: A solid-modeling, feature-based, web-enabled system for building parametric geometry." 21st AIAA Computational Fluid Dynamics Conference. 2013.

[15] Karman, Steve L., and Nicholas J. Wyman. "Automatic unstructured mesh generation with geometry attribution." AIAA Scitech 2019 Forum. 2019.

[16] Cambier, Laurent, Sébastien Heib, and Sylvie Plot. "The Onera elsA CFD software: input from research and feedback from industry." Mechanics & Industry 14.3 (2013): 159-174.

[17] Economon, Thomas D., et al. "SU2: An open-source suite for multiphysics simulation and design." *Aiaa Journal* 54.3 (2016): 828-846.

[18] Destarac, D. "Drag extraction from numerical solutions to the equations of fluid dynamics: the far-field philosophy." *Maîtrise de la traînée et de l'impact sur l'environnement, 43ème Congrès d'Aérodynamique Appliquée de la 3AF* (2008).

[19] A. Ko, W.H. Mason and B. Grossman, "Transonic Aerodynamic of a Wing/Pylon/Strut Juncture", 21st AIAA Applied Aerodynamics Conference, 23-26 June 2003, Orlando.

[20] Kulfan, Brenda M. "Universal parametric geometry representation method." *Journal of aircraft* 45.1 (2008): 142-158.

[21] J. Gauvrit-Ledogar, et al. "Multidisciplinary overall aircraft design process dedicated to blended wing body configurations." *2018 Aviation Technology, Integration, and Operations Conference*. 2018.

[22] F. Moens, "A L0 aerodynamic model for aircraft multidisciplinary design and optimization process", 3AF conference, 28-30 March 2022, Toulouse, France.

[23] Vanderplaats G. N., "DOT user's manual", version 4.20, 1995.

[24] Liebeck, Robert H. "Design of the blended wing body subsonic transport." Journal of aircraft 41.1 (2004): 10-25.

[25] Lyu, Zhoujie, and Joaquim RRA Martins. "Aerodynamic design optimization studies of a blended-wing-body aircraft." Journal of Aircraft 51.5 (2014): 1604-1617.

[26] Meheut, Michael, Aurelien Arntz, and Gerald Carrier. "Aerodynamic shape optimizations of a blended wing body configuration for several wing planforms." 30th AIAA Applied Aerodynamics Conference. 2012.

[27] Kawai, Ronald T., Douglas M. Friedman, and Leonel Serrano. Blended wing body (BWB) boundary layer ingestion (BLI) inlet configuration and system studies. No. NASA/CR-2006-214534. 2006.

[28] Carter, Melissa B., et al. "Designing and testing a blended wing body with boundary-layer ingestion nacelles." Journal of aircraft 43.5 (2006): 1479-1489.

[29] Kim, Hyoung Jin, and Meng-Sing Liou. "Optimal inlet shape design of n2b hybrid wing body configuration." 48th AIAA/ASME/SAE/ASEE Joint Propulsion Conference & Exhibit. 2012.

[30] A. T. Wick, J. R. Hooker and C. J. Hardin, C. H. Zeune, "Integrated Aerodynamic Benefits of Distributed Propulsion", AIAA 2015-1500, 2015.

## 8. Copyright Statement

The authors confirm that they, and/or their company or organization, hold copyright on all of the original material included in this paper. The authors also confirm that they have obtained permission, from the copyright holder of any third party material included in this paper, to publish it as part of their paper. The authors confirm that they give permission, or have obtained permission from the copyright holder of this paper, for the publication and distribution of this paper as part of the ICAS proceedings or as individual off-prints from the proceedings.